Multiplicative Noise Removal with Spatially Varying Regularization Parameters[*]

Fang Li[†], Michael K. Ng[‡], and Chaomin Shen[§]

Abstract. The Aubert–Aujol (AA) model is a variational method for multiplicative noise removal. In this paper, we study some basic properties of the regularization parameter in the AA model. We develop a method for automatically choosing the regularization parameter in the multiplicative noise removal process. In particular, we employ spatially varying regularization parameters in the AA model in order to restore more texture details of the denoised image. Experimental results are presented to demonstrate that the spatially varying regularization parameters method can obtain better denoised images than the other tested multiplicative noise removal methods.

Key words. multiplicative noise, total variation, textures, spatially varying regularization parameters

AMS subject classifications. 65F22, 65J22

DOI. 10.1137/090748421

1. Introduction. Given a noisy image $f(x,y) : \Omega \to \mathbb{R}$ $(f(x,y) > 0)$, where Ω is a bounded open subset of $\mathbb{R}^2$, we want to obtain a decomposition

$$(1.1) \qquad f(x,y) = u(x,y) \ n(x,y),$$

where $u(x,y)$ is the true image and $n(x,y)$ is the multiplicative noise. Unlike additive noise removal problems, a noisy image is formed by multiplication of noise and the original image, so almost all information of the original image may disappear in the observed image. The multiplicative noise arises in medical imaging, for instance, in magnetic field inhomogeneity in MRI [8] and speckle noise in ultrasound [2, 13], when a monochromatic radiation is scattered from a surface whose roughness is of the order of a wavelength, causing wave interference which results in speckle or multiplicative noise in an image. This phenomenon usually arises in laser, microscope, and synthetic aperture radar (SAR) images [12].

Aubert and Aujol [3] derived a model from maximum a posterior (MAP) estimation under the assumption that the multiplicative noise follows a Gamma distribution. They aimed to minimize the following energy:

$$(1.2) \qquad E_\lambda(u) = \int_\Omega |\nabla u| + \lambda \int_\Omega \left(\log u + \frac{f}{u} \right),$$

[†]Department of Mathematics, East China Normal University, Shanghai 200062, China (lifangswnu@126.com).

[‡]Corresponding author. Centre for Mathematical Imaging and Vision and Department of Mathematics, Hong Kong Baptist University, Kowloon Tong, Hong Kong (mng@math.hkbu.edu.hk).

[§]Department of Computer Science, East China Normal University, Shanghai 200062, China (cmshen@cs.ecnu.edu.cn).

where λ is a positive constant parameter to balance the regularization term (the first term on the right-hand side) and the fidelity term (the second term on the right-hand side). Numerical results have shown that this algorithm can perform quite well for cartoon images (piecewise constant regions). In [7], Huang, Ng, and Wen proposed a new total variation (TV) method for multiplicative noise removal based on the Aubert–Aujol (AA) model.

We note that the use of the TV regularization $\int_\Omega |\nabla u|$ for Gaussian noise removal was first proposed and developed by Rudin, Osher, and Fatemi [10]. In the bounded variation space [3], TV $\int_\Omega |\nabla u|$ is defined as

$$\int_\Omega |\nabla u| := \sup \left\{ \int_\Omega u\,\mathrm{div}\varphi \mid \varphi \in C_c^1(\Omega, \mathbb{R}^2), \ |\varphi| \le 1 \right\}.$$

Other variational methods for multiplicative noise removal are considered and studied in [9, 11]. In [9], Rudin, Lions, and Osher assumed that there is some prior information about the mean and the variance of the multiplicative noise:

$$(1.3) \qquad \int_\Omega (n-1) = 0 \quad \text{and} \quad \int_\Omega (n-1)^2 = |\Omega|\sigma^2,$$

where $|\Omega|$ denotes the area of Ω. This states that the mean of the noise is equal to 1, and the variance is equal to σ^2. They proposed to minimize the TV norm

$$E(u) = \int_\Omega |\nabla u|$$

subject to the constraints

$$(1.4) \qquad \int_\Omega \left(\frac{f}{u} - 1\right) = 0 \quad \text{and} \quad \int_\Omega \left(\frac{f}{u} - 1\right)^2 = |\Omega|\sigma^2.$$

The gradient projection method leads to the following evolution equation:

$$\frac{\partial u}{\partial t} = \mathrm{div}\left(\frac{\nabla u}{|\nabla u|}\right) + \lambda_1 \frac{f}{u^2} + \lambda_2 \frac{f^2}{u^3},$$

where the two Lagrange multipliers λ_1 and λ_2 are solved by requiring that

$$\frac{\partial}{\partial t} \int_\Omega \frac{f}{u} = -\int_\Omega \frac{f}{u^2} \frac{\partial u}{\partial t} = 0,$$

$$\frac{\partial}{\partial t} \int_\Omega \left(\frac{f}{u} - 1\right)^2 = -2\int_\Omega \frac{f^2}{u^3} \frac{\partial u}{\partial t} = 0.$$

Explicitly, λ_1 and λ_2 can be given by

$$\lambda_1 = \frac{\begin{bmatrix} -\int \frac{f}{u^2}\mathrm{div}\left(\frac{\nabla u}{|\nabla u|}\right) & \int \frac{f^3}{u^5} \\ -\int \frac{f^2}{u^3}\mathrm{div}\left(\frac{\nabla u}{|\nabla u|}\right) & \int \frac{f^4}{u^6} \end{bmatrix}}{\begin{bmatrix} \int \frac{f^2}{u^4} & \int \frac{f^3}{u^5} \\ \int \frac{f^3}{u^5} & \int \frac{f^4}{u^6} \end{bmatrix}}, \qquad \lambda_2 = \frac{\begin{bmatrix} \int \frac{f^2}{u^4} & -\int \frac{f}{u^2}\mathrm{div}\left(\frac{\nabla u}{|\nabla u|}\right) \\ \int \frac{f^3}{u^5} & -\int \frac{f^2}{u^3}\mathrm{div}\left(\frac{\nabla u}{|\nabla u|}\right) \end{bmatrix}}{\begin{bmatrix} \int \frac{f^2}{u^4} & \int \frac{f^3}{u^5} \\ \int \frac{f^3}{u^5} & \int \frac{f^4}{u^6} \end{bmatrix}}.$$

Recently, Shi and Osher [11] considered the log of both sides of (1.1) which converts the multiplicative problem into the additive one. They generalized the nonlinear relaxed inverse scale space (RISS) method to the transformed additive problem. The numerical results show a very good denoising effect and significant improvement over earlier multiplicative models [9].

Recently, Durand, Fadili, and Nikolova [5] proposed a method composed of several stages for multiplicative noise removal. They use the log-image data, employ a reasonable under-optimal hard-thresholding on the curvelet transform coefficients of the log-image data, and then apply a variational method where they minimize a specialized criterion composed of an l_1-norm data-fitting to the threshold coefficients and a TV term in the image domain. Their restored images combine the advantages of shrinkage and variational methods. Their numerical results outperform the AA model and the Stein–Block denoising method. In their proposed method, they also need to select suitable regularization parameters to reach the good level of performance.

In this paper, we first study some basic properties of the regularization parameter in the AA model. In order to overcome the difficulty in choosing an optimal parameter λ for the AA model, we develop a method for automatically choosing the regularization parameter λ. Based on the idea of the paper in [6], we further introduce a spatially varying fidelity term in the multiplicative denoising model so that both cartoon-like and texture information in the multiplicative noise denoising process can be much better preserved. Here we replace the constant λ (the global fidelity coefficient) in the AA model by local fidelity coefficients $\lambda(x)$, $x \in \Omega$. We derive a formula for computing such coefficients $\lambda(x)$ automatically. Experimental results are presented to demonstrate that spatially varying regularization parameters can obtain better denoised images than the other tested multiplicative noise removal methods.

This paper is organized as follows. In section 2, we study the role of the fidelity parameter in the AA model. In section 3, we develop a regularization parameter selection scheme for multiplicative noise removal. In section 4, we consider and study spatially varying regularization parameters for the AA model. In section 5, experimental results are reported.

2. The regularization parameter. In this section, we study some basic properties needed to understand the role of the regularization parameter λ in the AA model. Here we assume that $f \in L^\infty(\Omega)$. Let u_λ be a minimizer of $E_\lambda(u)$; see [3] for the proof of the existence of a minimizer for the AA model. For the multiplicative noise removal problem, we use $\frac{f}{u_\lambda}$ to represent the residue. Let us define the operator

$$T_\lambda : L^\infty(\Omega) \to L^\infty(\Omega)$$

by $T_\lambda(f) = u_\lambda$. We know that u_λ necessarily satisfies the Euler–Lagrange equation:

$$(2.1) \qquad \operatorname{div}\left(\frac{\nabla u_\lambda}{|\nabla u_\lambda|}\right) + \lambda\left(\frac{f - u_\lambda}{u_\lambda^2}\right) = 0,$$

with Neumann boundary condition $\frac{\partial u_\lambda}{\partial \vec{N}} = 0$, where $\vec{N}$ denotes the unit outward normal of boundary $\partial\Omega$. It is straightforward to show the following properties of λ.

Property 1. $T_\lambda(c) = c$ and $T_{c\lambda}(cf) = cT_\lambda(f)$, where c is a positive constant.

Proof. Let $f = c > 0$. Since the term $\int_\Omega \left(\log u + \frac{f}{u} \right)$ attains its minimum at $u = f = c$ and $\int_\Omega |\nabla c| = 0$, we get that $u = c$ is the minimizer. For a general image f, we have

$$T_\lambda(f) = u_\lambda = \arg\min \left\{ E(u) = \int_\Omega |\nabla u| + \lambda \int_\Omega \left(\log u + \frac{f}{u} \right) \right\}.$$

Since

$$\frac{1}{c} \left\{ \int_\Omega |\nabla(cu_\lambda)| + c\lambda \int_\Omega \left(\log(cu_\lambda) + \frac{cf}{cu_\lambda} \right) \right\} = \int_\Omega |\nabla u_\lambda| + \lambda \int_\Omega \left(\log c + \log u_\lambda + \frac{f}{u_\lambda} \right),$$

we obtain

$$cu_\lambda = \arg\min \left\{ \int_\Omega |\nabla u| + c\lambda \int_\Omega \left(\log u + \frac{cf}{u} \right) \right\}.$$

Hence we get the result

$$T_{c\lambda}(cf) = cu_\lambda = cT_\lambda(f). \qquad \blacksquare$$

Property 2. *The L^∞ norm of u_λ is bounded by a constant dependent only on the initial data f.*

Proof. This result follows immediately from the theorem in [3] since the solution of (2.1) satisfies the maximum principle,

$$0 < \inf_\Omega f \le u_\lambda \le \sup_\Omega f. \qquad \blacksquare$$

Property 3. *The sequence u_λ converges strongly in $L^1(\Omega)$ to the average of the initial data f as $\lambda \to 0$; the sequence u_λ converges to f almost everywhere (a.e.) as $\lambda \to +\infty$.*

Proof. Since u_λ is a minimizer of $E_\lambda(u)$, we have for each $v \in BV(\Omega)$

$$(2.2) \qquad \int_\Omega |\nabla u_\lambda| + \lambda \int_\Omega \left(\log u_\lambda + \frac{f}{u_\lambda} \right) \le \int_\Omega |\nabla v| + \lambda \int_\Omega \left(\log v + \frac{f}{v} \right).$$

Setting $v = 1$ in (2.2) and using the fact that $\int_\Omega \left(\log u + \frac{f}{u} \right)$ attains its minimum at $u = f$, we get

$$\int_\Omega |\nabla u_\lambda| + \lambda \int_\Omega (\log f + 1) \le \int_\Omega |\nabla u_\lambda| + \lambda \int_\Omega \left(\log u_\lambda + \frac{f}{u_\lambda} \right) \le \lambda \int_\Omega f.$$

Then

$$0 \le \int_\Omega |\nabla u_\lambda| \le \lambda \int_\Omega (f - \log f - 1) \to 0 \ (\lambda \to 0).$$

Hence

$$\lim_{\lambda \to 0} \int_\Omega |\nabla u_\lambda| = 0.$$

Thanks to the Poincaré-Wirtinger inequality,

$$(2.3) \qquad \int_\Omega |u_\lambda - \overline{u_\lambda}| \le C \int_\Omega |\nabla u_\lambda| \to 0 \ (\lambda \to 0),$$

where $\overline{u_\lambda}$ is the average of u_λ. Since $\overline{u_\lambda}$ is a constant and $\int_\Omega |\nabla \overline{u_\lambda}| = 0$, the problem of minimizing $E_\lambda(u)$ as $\lambda \to 0$ is equivalent to minimizing

$$F(\overline{u_\lambda}) = \int_\Omega \left(\log \overline{u_\lambda} + \frac{f}{\overline{u_\lambda}} \right).$$

Taking the derivative of F with respect to $\overline{u_\lambda}$ and setting the result to zero gives

$$\int_\Omega \left(\frac{1}{\overline{u_\lambda}} - \frac{f}{\overline{u_\lambda}^2} \right) = 0 \ (\lambda \to 0).$$

Then $\lim_{\lambda \to 0} \overline{u_\lambda} = \overline{f}$, where $\overline{f}$ is the average of f. Together with (2.3) we conclude that u_λ converges strongly in $L^1(\Omega)$ to the average of the observed image f as λ goes to zero.

To prove the second part, by (2.2), we have

$$\int_\Omega |\nabla u_\lambda| + \lambda \int_\Omega \left(\log u_\lambda + \frac{f}{u_\lambda} \right) \leq \int_\Omega |\nabla f| + \lambda \int_\Omega (\log f + 1).$$

Then as $\lambda \to +\infty$,

$$\int_\Omega \left(\log u_\lambda + \frac{f}{u_\lambda} \right) \leq \frac{1}{\lambda} \int_\Omega |\nabla f| + \int_\Omega (\log f + 1) \to \int_\Omega (\log f + 1).$$

Hence we have

$$\int_\Omega \left(\frac{f}{u_\lambda} - \log \frac{f}{u_\lambda} - 1 \right) \to 0 \ (\lambda \to +\infty).$$

It is easy to show that the function $F(u) = \int_\Omega (u - \log u - 1)$ is convex, attaining its minimum 0 at $u = 1$. Then we can deduce that

$$\lim_{\lambda \to +\infty} u_\lambda = f \quad \text{a.e. } x \in \Omega. \qquad \blacksquare$$

Next we consider and study the data fidelity term

$$h(\lambda) \equiv \int_\Omega \left(\log u_\lambda + \frac{f}{u_\lambda} \right).$$

Here we use the notation $J(u_\lambda) := \int_\Omega |\nabla u_\lambda|$. We can show the following property.

Property 4. *Assume f is not a constant. Then the function $h(\lambda)$ is a strictly decreasing function.*

Proof. Consider first $\lambda > \mu \geq 0$. We have

(2.4) $$J(u_\lambda) + \lambda h(\lambda) \leq J(u_\mu) + \lambda h(\mu),$$

(2.5) $$J(u_\mu) + \mu h(\mu) \leq J(u_\lambda) + \mu h(\lambda).$$

Combining both inequalities, we get $(\lambda - \mu) h(\lambda) \leq (\lambda - \mu) h(\mu)$, and this inequality shows that $h(\cdot)$ is nonincreasing. Next we want to prove that the mapping is strictly decreasing. Suppose there exists $\lambda < \mu$ such that $h(\lambda) = h(\mu)$. Since h is nonincreasing, we have $h(\tau) = h(\lambda)$ for

any $\tau \in [\lambda, \mu]$. In (2.4) and (2.5), we find that $J(u_\lambda) = J(u_\mu)$. Therefore we derive that u_τ is a minimizer of energy (1.2) for any $\tau \in [\lambda, \mu]$. This means that

$$0 \in \partial J(u_\tau) - \tau \left(\frac{f - u_\tau}{u_\tau^2} \right) \quad \forall \tau \in [\lambda, \mu].$$

Remember that $p \in \partial J(u_\tau)$ is equivalent to $\langle p, u_\tau \rangle = J(u_\tau) + J^*(p)$, where J^* is the Legendre–Fenchel transform of the convex function J. Here $J^*(p) = \chi_V(p)$ ($= 0$ if $p \in V$ or $+\infty$ if $p \notin V$), where V is a convex closed set (the closure of $\{\text{div}\phi : \phi \in C_c^\infty(\Omega) \text{ and } \|\phi\|_\infty \leq 1\}$). Therefore we obtain

$$\tau \int_\Omega \left(\frac{f - u_\tau}{u_\tau^2} \right) u_\tau = J(u_\tau) \quad \forall \tau \in [\lambda, \mu],$$

which implies that $J(u_\tau) = 0$ and u_τ is a constant. Hence f is a constant. This is a contradiction to our assumption that f is not a constant image. Then we conclude that the function $h(\lambda)$ must be a strictly decreasing function. ■

We use a toy image to test the AA model with different values of the parameter λ to demonstrate the above properties. Figure 1(a) shows the noise-free image. In Figure 1(b), it is contaminated by multiplicative Gaussian noise with mean 1 and variance 0.01. We take Figure 1(b) as the given data f in the AA model. Table 1 and Figure 1(c) demonstrate the following properties of the parameter λ in the AA model: As λ goes to 0, u_λ goes to a constant, with almost all the textures and details contained in the residue part. Then as λ increases from zero to 1000, the solution contains more structure and textures, while the residue part contain less useful information. It seems that a good balance is achieved at about $\lambda = 10^3$. However, when λ becomes larger, the solution contains more details, including the noise. At $\lambda = 10^4$, the solution seems very noisy like the given image Figure 1(b). We expect that as λ goes to infinity, u_λ goes to f. We observe that the signal-to-noise ratio (SNR) as a function of λ reaches a maximum point at $\lambda \approx 1500$ and then decreases. Here SNR is defined as

$$\text{SNR} = 10 \cdot \log_{10} \left(\frac{\int_\Omega (I - \bar{I})^2}{\int_\Omega (n - \bar{n})^2} \right),$$

where I denotes the noise-free image, n denotes the noise, $\bar{I} = \int_\Omega I / |\Omega|$, and $\bar{n} = \int_\Omega n / |\Omega|$.
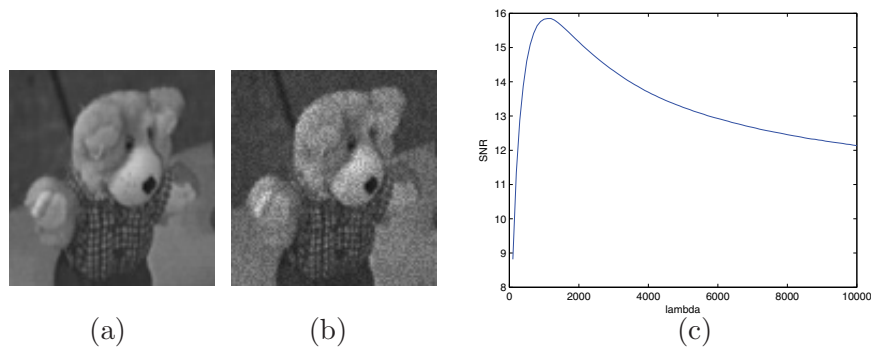

(a) (b) (c)
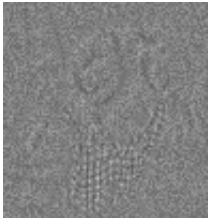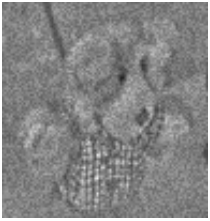
Figure 1. (a) *The toy image;* (b) *the noisy image;* (c) *SNR for the denoised toy image using the AA model with different values of* λ.

Table 1
The solution u_λ of the AA model and the residual for different values of λ.

λ	Solution u_λ	Residue f/u_λ	λ	Solution u_λ	Residue f/u_λ
0			500		
10			10^3		
100			10^4		

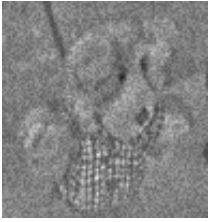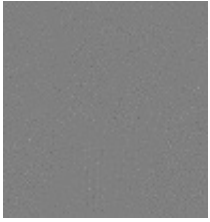In the AA model (1.2), λ is a constant. According to the above properties, it is not easy to choose an optimal parameter λ for multiplicative noise removal. With a small λ, the solution of the AA model will lose many details and cause the denoised image to be over-smooth, while with a large λ, the noise appears in the image solution. In the next section, we are interested in developing a method for automatically selecting a suitable value of λ such that we can obtain the high quality of denoised images.

3. The selection of the scalar regularization parameter. Following [9, 11], we assume that we have some prior information about the mean and variance of the multiplicative noise; see (1.4). We first study how to find the scalar regularization parameter λ automatically for the AA model.

We consider the AA model as follows:

$$(3.1) \qquad \min\left\{ E(u,\lambda) = \int_\Omega |\nabla u| + \lambda \int_\Omega \left(\log u + \frac{f}{u} \right) \right\},$$

where λ is a scalar variable. Then the corresponding Euler–Lagrange equation for u is given in the same formulation as in (2.1). By multiplying (2.1) with $(u - f)$ and integrating on the

image domain Ω, we obtain

$$\int_\Omega \operatorname{div}\left(\frac{\nabla u}{|\nabla u|}\right)(u - f) - \lambda \int_\Omega \left(\frac{f}{u} - 1\right)^2 = 0.$$

Using the prior information (1.4), the scalar λ can be computed by

$$(3.2) \qquad \lambda = \frac{1}{|\Omega|\sigma^2} \int_\Omega \operatorname{div}\left(\frac{\nabla u}{|\nabla u|}\right)(u - f).$$

Then the solution of (3.1) is obtained by evolving the negative gradient flow

$$(3.3) \qquad \frac{\partial u}{\partial t} = \operatorname{div}\left(\frac{\nabla u}{|\nabla u|}\right) + \lambda \left(\frac{f - u}{u^2}\right)$$

with Neumann boundary condition and updating λ by (3.2) iteratively until convergence. We note that the above formula for λ is different from that given in [9]. In section 5, we will present the denoising results by using the above alternating updating method.

4. Spatially varying regularization parameters. We note in (3.1) that λ is just a weighting parameter for balancing the regularization term and the fidelity term. The regularization term requires that the image be smooth, and the fidelity term requires that the useful information in the noisy image f be retained. As shown as in Table 1, as λ increases, the cartoon structure is separated out from the given noisy image f in the first place, and then the texture part is separated out. It is clear that a small λ can be used for denoising cartoon regions, while a large λ can be used for denoising texture regions. Since there are many features in an image such as cartoon, textures, and small details, a global constant parameter λ may not be suitable for all the image features. Hence a spatially varying regularization parameter function $\lambda(x, y)$ will be useful in order to restore different features in the denoising process. In [1, 4], local constraints for Gaussian noise removal have been used to determine spatially varying regularization parameters such that high-quality denoised images are obtained. Here we adapt the idea in [6] which considers only additive Gaussian noise removal.

In order to understand the image features locally, we compute the local mean data fidelity. We make use of the two-dimensional Gaussian kernel in the calculation:

$$E_{ava}(u)(x, y) = \int_\Omega K(w - x, z - y)\left(\log u(w, z) + \frac{f(w, z)}{u(w, z)}\right)dwdz,$$

where K is a symmetric Gaussian kernel with $\int_\Omega K(x, y) = 1$. Now the multiplicative denoising model is given by

$$\min\left\{E(u, \lambda) = \int_\Omega |\nabla u| + \int_\Omega \lambda E_{ava}(u)\right\}.$$

We remark that λ is a function of x and y in the above model. By using the symmetry of K,

i.e., $K(w - x, z - y) = K(x - w, y - z)$, we obtain

$$
\begin{aligned}
&\int_\Omega \lambda(x,y) E_{ava}(u)(x,y) dxdy \\
&= \int_\Omega \lambda(x,y) \left(\int_\Omega K(w-x, z-y) \left(\log u(w,z) + \frac{f(w,z)}{u(w,z)} \right) dwdz \right) dxdy \\
&= \int_\Omega \int_\Omega \lambda(w,z) K(x-w, y-z) \left(\log u(x,y) + \frac{f(x,y)}{u(x,y)} \right) dxdydwdz \\
&= \int_\Omega \left(\int_\Omega K(x-w, y-z) \lambda(w,z) dwdz \right) \left(\log u(x,y) + \frac{f(x,y)}{u(x,y)} \right) dxdy \\
&= \int_\Omega (K*\lambda)(x,y) \left(\log u(x,y) + \frac{f(x,y)}{u(x,y)} \right) dxdy.
\end{aligned}
$$

Then the denoising model can be rewritten as

$$
\min \left\{ E(u,\lambda) = \int_\Omega |\nabla u| + \int_\Omega K * \lambda \left(\log u + \frac{f}{u} \right) \right\}.
$$

The Euler–Lagrange equation for u is

$$
(4.1) \qquad\qquad -\operatorname{div}\left(\frac{\nabla u}{|\nabla u|} \right) + K * \lambda \left(\frac{u-f}{u^2} \right) = 0.
$$

By using the same strategy as in the previous section, we have

$$
\int_\Omega \operatorname{div}\left(\frac{\nabla u}{|\nabla u|} \right) (u - f) = \int_\Omega K * \lambda \left(\frac{f}{u} - 1 \right)^2.
$$

Again using the symmetry property of K, a sufficient condition for the above equality is

$$
\operatorname{div}\left(\frac{\nabla u}{|\nabla u|} \right) (u - f) = \lambda K * \left(\frac{f}{u} - 1 \right)^2.
$$

Thus the function $\lambda(x,y)$ can be calculated as follows:

$$
(4.2) \qquad\qquad \lambda(x,y) = \frac{D(x,y)}{V(x,y)} \quad \forall (x,y) \in \Omega,
$$

where $D(x,y) = \operatorname{div}(\frac{\nabla u}{|\nabla u|})(u-f)$ and $V(x,y) = K*(\frac{f}{u}-1)^2$. Then the solution is obtained by evolving the negative gradient flow for the Euler–Lagrange equation in (4.1), updating $\lambda(x,y)$ by (4.2) iteratively until convergence. Since there may be too many variables $u(x,y)$ and $\lambda(x,y)$ to be updated, this process is very sensitive to the initial choice of u or λ. According to our numerical experience, the denoising results may not be promising.

Inspired by [6], we note that $V(x,y)$ is related to the local variance of the multiplicative noise, which can be approximated by

$$
(4.3) \qquad\qquad V(x,y) \approx \frac{\sigma^4}{K * (r - \bar{r})^2},
$$

where $r = \frac{f}{\hat{u}} - 1$, $\bar{r}$ is the local mean of r, and $\hat{u}$ is an approximation of the original image. Such an approximation can be obtained by preprocessing the noisy image by using the AA model or the AA model with automatic selection of regularization parameter (3.1).

Let us study the property of $V(x, y)$ defined in (4.3). Assume that a noise-free image is decomposed as follows: $u = u_c + u_t$, where $u_c > 0$ and $u_t > 0$ represent the cartoon part and the texture part of the image, respectively. Then $f = un = (u_c + u_t)n$. If the image is cartoon-like (i.e., u_t is close to 0), then the model using the scalar regularization parameter can give high-quality denoising results such that $\hat{u} \approx u_c = u$ and the noise residue $n \approx \frac{f}{\hat{u}}$. By assumption (1.4), the local variance in this case is almost a global constant; i.e., $LV(x, y) = \sigma^2$ for $(x, y) \in \Omega$, where LV denotes local variance. Therefore, we have $V(x, y) = \sigma^2$ for $(x, y) \in \Omega$. Then the spatially varying regularization parameters method becomes the AA model with automatic selection of regularization parameter, which works quite well for cartoon-like images.

In the case of images with textures (most natural images belong to this type), some textures as well as noise will be smoothed and included in the residue $\frac{f}{\hat{u}}$. The AA model with automatic selection of regularization parameter gives a cartoon-like image which is $\hat{u} \approx u_c$. We obtain

$$\frac{f}{\hat{u}} - 1 \approx \frac{(u_c + u_t)n}{u_c} - 1 = \left(1 + \frac{u_t}{u_c}\right)n - 1.$$

Then the local variance of $\frac{f}{\hat{u}} - 1$ is equal to

$$LV\left(\frac{f}{\hat{u}} - 1\right) = LV\left(\left(1 + \frac{u_t}{u_c}\right)n\right).$$

For the regions of texture in the image, u_t/u_c is greater than 0. It follows that

$$V(x, y) = \frac{\sigma^4}{LV\left(\left(1 + \frac{u_t}{u_c}\right)n\right)} < \sigma^2.$$

Then by (4.2), the local fidelity coefficients in texture regions are larger than those in the cartoon regions. It implies that the texture regions are less smoothed than the cartoon regions and that more texture details of the denoised image can be restored.

As a summary, the proposed algorithm is to evolve the negative gradient flow

$$(4.4) \qquad \frac{\partial u}{\partial t} = \text{div}\left(\frac{\nabla u}{|\nabla u|}\right) + K * \lambda\left(\frac{f - u}{u^2}\right)$$

and update λ by (4.2) and (4.3) until convergence. We find in numerical results that this approach is more effective.

In the next section, we will test the performance of the AA model with automatic selection of regularization parameter (section 3) and the spatially varying regularization parameters method (section 4) and make a comparison with existing multiplicative denoising techniques.

5. Experimental results. We perform the AA model [3], the AA model with automatic selection of regularization parameter (section 3), and the spatially varying regularization parameters method (section 4) for multiplicative noise removal. In addition, we compare these with other TV-based models [7, 9, 11] for multiplicative noise removal. In the tests, we set as the stopping criterion of their iterative schemes that the mean value of $|u^{(k)} - u^{(k-1)}|$ should be less than a small number defined by the user such as 0.01, where $u^{(k)}$ is the iterate of the scheme. In the tests, we consider the multiplicative noise in each pixel following Gamma distribution of mean one with its probability density function given by

$$(5.1) \qquad \mathrm{pdf}(n) = \begin{cases} \dfrac{L^L n^{L-1}}{\Gamma(L)} e^{-Ln}, & n > 0, \\ 0, & n \leq 0, \end{cases}$$

where $\Gamma(\cdot)$ is a Gamma function. The variance of Gamma distribution is given by $1/L$. When L is small, the noise is more serious. In the experiments, the variances of Gamma noise are set to be 0.01, 0.03, 0.05, and 0.1, respectively.

In order to quantify the denoising performance, we compare the SNRs of the denoised images for different models in Tables 2–3. In the tables, "AA," "Scalar," "Spatial," "RLO," "RISS," "HNW," "ROF," and "ATV" represent the AA model, the AA model with automatic selection of regularization parameter, the spatially varying parameters method, the Rudin–Lions–Osher TV model in [9], the nonlinear relaxed inverse scale space method in [11], the Huang–Ng–Wen method in [7], the Rudin–Osher–Fatemi model [10], and the adaptive TV model in [6], respectively. In the proposed spatially varying parameters method, the radius of the Gaussian kernel is set to be 3. Note that the four methods Scalar, Spatial, RLO, and ATV are automatic parameter models. The others are manual parameter models; for example, AA, ROF, and RISS require one parameter (the fidelity coefficient λ) input, and HNW involves two input parameters in the model. One parameter is for the regularization, and the other is for the closeness between the two denoised images. For simplicity, we set the closeness parameter to be very large. We deal with only one regularization parameter in the HNW method. We perform the manual parameter selection using different values of parameters and pick up the highest SNR denoising result among all the tested values.

Table 2
Comparison of SNRs (in dB) of the different models for Gamma noises with variance 0.01.

Image	Noisy	AA	Scalar	Spatial	RLO	RISS	HNW	ROF	ATV
Mosaic	10.99	13.19	12.19	13.95	12.48	13.41	13.87	12.80	13.15
Lena	11.05	17.85	17.55	17.99	17.60	17.25	17.74	16.88	15.47
Barbara	12.18	15.64	14.60	16.29	15.55	16.18	16.08	15.10	14.21

When the noise variance is 0.01, it is clear from Table 2 that the spatially varying parameters method has the highest SNR among all the tested methods for all tested images. For such a low-noise level, we find that the performances of ROF and ATV (they are the denoising models for additive noise) are not good.

In Table 3, we further show the denoising results using different methods when the noise variance is higher. We find in the table that when the noise variance is 0.03, 0.05, and 0.1,

Table 3
Comparison of SNRs (in dB) of the different models for Gamma noises with variances 0.03, 0.05, *and* 0.1.

Image	Noise variance	Noisy	AA	Scalar	Spatial	RLO	RISS	HNW
Mosaic	0.03	6.30	9.56	8.99	10.64	9.37	10.45	10.21
	0.05	4.07	7.98	7.72	8.90	8.09	8.68	8.62
	0.1	1.04	6.08	6.16	6.83	6.29	6.65	6.75
Lena	0.03	6.29	14.90	14.76	15.07	15.07	15.02	14.90
	0.05	4.07	13.56	13.53	13.78	13.73	13.62	13.59
	0.1	1.07	11.68	11.76	12.08	12.07	11.98	11.97
Barbara	0.03	7.50	12.75	12.12	13.29	12.83	11.24	13.14
	0.05	5.31	11.39	11.07	11.92	11.38	11.89	11.88
	0.1	2.28	9.84	9.82	10.31	9.90	10.25	10.29

the spatially varying parameters method can give better denoising images in terms of SNRs than the other methods.

Next we show the denoised images in Figures 2, 4, and 5 corresponding to the denoising results in Table 2. Figures 2(a), 4(a), and 5(a) show the original images. Figures 2(b), 4(b), and 5(b) show the noisy images. In Table 2, we have reported that the spatially varying parameters method gives the best denoising results in terms of SNRs. We will see from the figures that the visual quality of the denoised images by the spatially varying parameters method is also very good.

In Figure 2(a), we note that the pixel values are constant in the upper left and bottom right regions of the image (they are called cartoon regions). Figures 2(c) and 2(d) are the denoised images by using the AA model with optimal λ (the trial-and-error approach) and the AA model with automatic selection of regularization parameter (section 3). In Figures 2(c) and 2(d), we see that there are many undesirable blocky artifacts in the cartoon regions by using the AA model and the AA model with automatic selection of regularization parameter. Figure 2(f) shows the function $\lambda(x,y)$ in the spatially varying parameters method, and the function values show the two texture regions. Based on such detection, the spatially varying parameters method gives more pleasing results in Figure 2(e). In Figures 2(g) and 2(h), we also show the results by using the ROF and the ATV additive denoising models. We see from these figures that the bottom right cartoon parts are still very noisy. We remark in the multiplicative noise case that the high-intensity region (such as the bottom right part of the mosaic) are more seriously contaminated by noise than those in the low-intensity region. In Figure 3, we show the noise residues for different methods. Again, it is clear that the spatially varying parameters method contains fewer useful textures than the other models.

In Figure 4, we show the denoising results of the Lena image. In Figure 4(c), we display the spatially varying parameters $\lambda(x,y)$ which can detect the textures on the hair and hat of the Lena image. We see from Figure 4(f) that the textures on the hair and hat are slightly better preserved. Also it is clear from Figures 4(g)–4(i) that the noise residue of the spatially varying parameters method contains fewer textures than the residues of the other models. Actually, since the Lena image contains a more cartoon-like structure, all the multiplicative denoising models can give good results; see Table 2 for the SNR comparison.

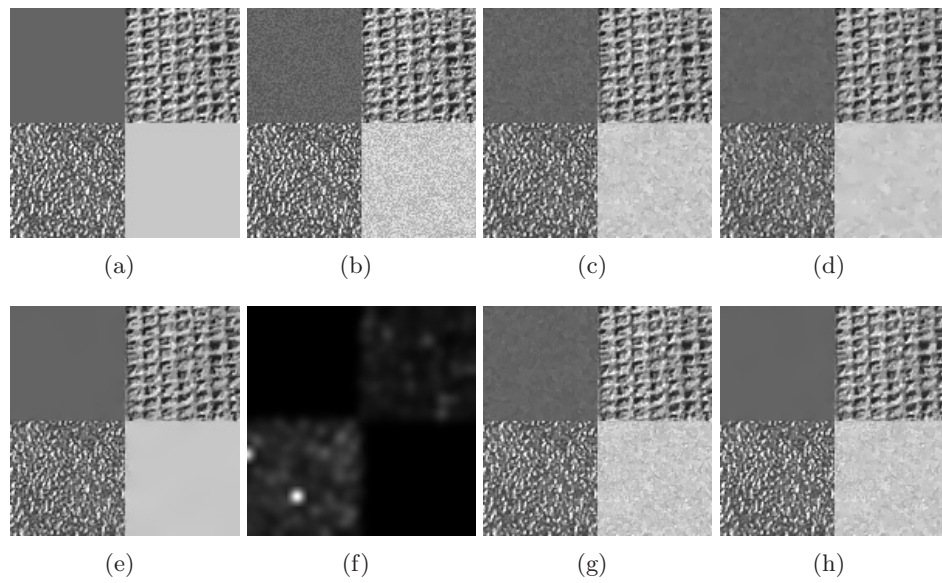In Figure 5(c), we display the spatially varying parameters $\lambda(x,y)$ which can detect the

(a)   (b)   (c)   (d)

(e)   (f)   (g)   (h)

Figure 2. (a) *The original synthetic image;* (b) *the noisy image;* (c) *the AA model with* $\lambda = 4600$; (d) *the AA model with automatic selection of parameter;* (e) *the spatially varying parameters method;* (f) $\lambda(x, y)$ *computed by the spatially varying parameters method;* (g) *the ROF model with* $\lambda = 4600$; (h) *the ATV model in* [5].
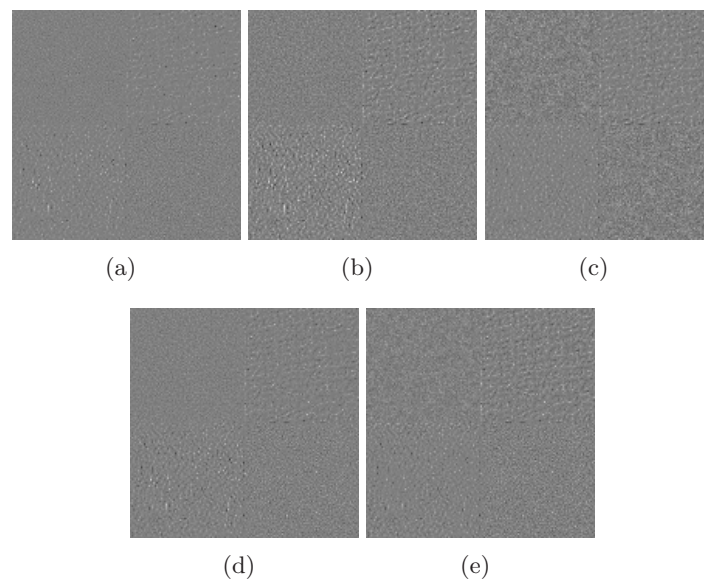

(a)   (b)   (c)

(d)   (e)

Figure 3. *The noise residue:* (a) *the AA model;* (b) *the AA model with automatic selection of parameter;* (c) *the spatially varying parameters method;* (d) *the ROF model;* (e) *the ATV model.*
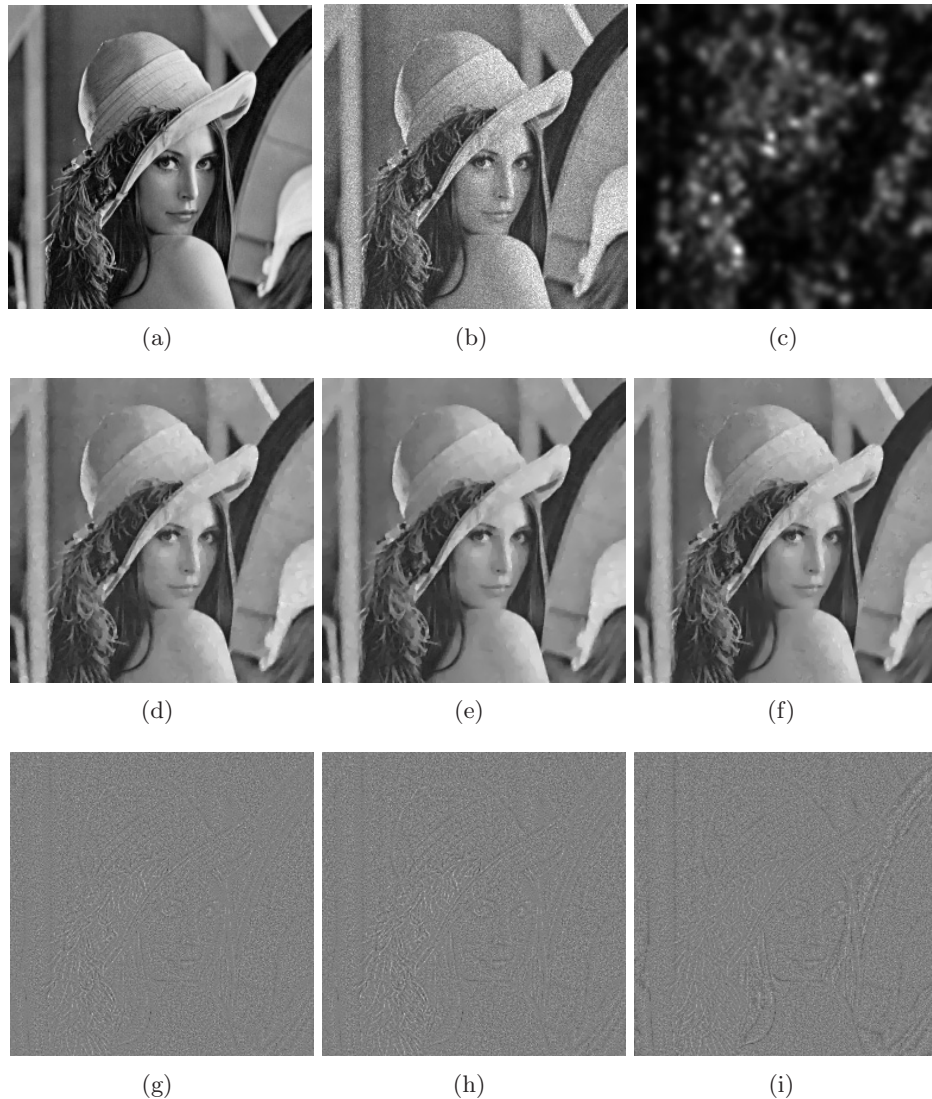
Figure 4. (a) *The original "Lena" image;* (b) *the noisy image;* (c) $\lambda(x, y)$ *computed by the spatially varying parameters method;* (d) *the AA model with* $\lambda = 900$; (e) *the AA model with automatic selection of parameter;* (f) *the spatially varying parameters method;* (g) *the noise residue of the AA model;* (h) *the noise residue of the the AA model with automatic selection of parameter;* (i) *the noise residue of the spatially varying parameters method.*

textures on the scarf of the Barbara image. The spatially varying parameters method gives a better results as a whole in Figure 5(f). For a detailed comparison, we give in Figures 6 and 7 the zoomed versions of two parts of the Barbara image. It is clear from Figure 5 that the spatially varying parameters method preserves the textures as well as the other models (AA, RLO, RISS, HNW) except the AA model with automatic selection of regularization parameter. The AA model with automatic selection of regularization parameter over-smoothes the textures on the scarf. However, the four methods require us to determine suitable regu-

Figure 5. (a) *The original "Barbara" image, the marked rectangles are marked for zooming;* (b) *the noisy image;* (c) $\lambda(x,y)$ *computed by the spatially varying parameters method; the denoised images:* (d) *the AA model with* $\lambda = 1900$; (e) *the AA model with automatic selection of parameter;* (f) *the spatially varying parameters method;* (g) *the RLO model;* (h) *the RISS model with* $\lambda = 10$; (i) *the HNW model with* $\lambda = 6$.

larization parameters. The proposed method can determine the spatially varying parameters automatically. In Figure 8, we find that the cartoon parts are better preserved by the AA model with automatic selection of regularization parameter and the proposed spatially varying parameters method than by other models (in which some noises are retained). Again we find in Figure 5 that the noise residue of the spatially varying parameters method contains fewer textures for the scarf than the residues of the other models. The results of the ROF and the ATV models are not displayed since their denoising results are not good; see Table 2 for the SNR comparison.
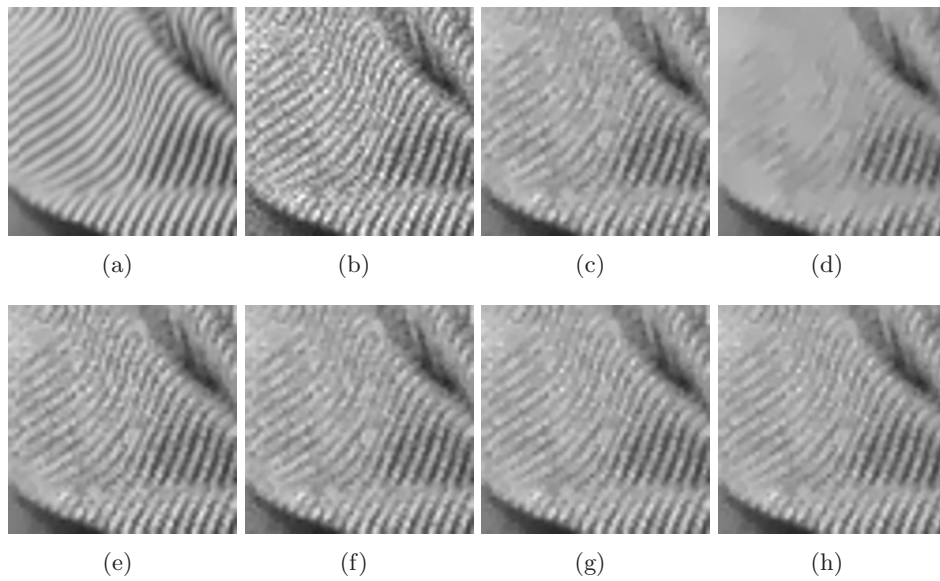
(a)   (b)   (c)   (d)

(e)   (f)   (g)   (h)

Figure 6. (a) *The zoomed version of the Barbara image in Figure* 5(a); (b) *the corresponding noisy part;* (c) *the AA model;* (d) *the AA model with automatic selection of parameter;* (e) *the spatially varying parameters method;* (f) *the RLO model;* (g) *the RISS model;* (h) *the HNW model.*
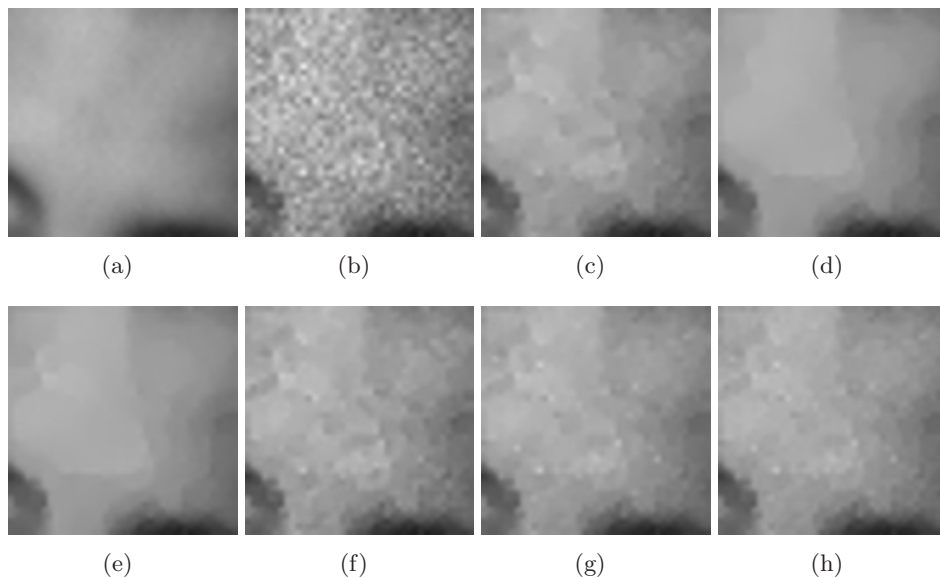

(a)   (b)   (c)   (d)

(e)   (f)   (g)   (h)

Figure 7. (a) *The zoomed version of the Barbara image in Figure* 5(a); (b) *the corresponding noisy part;* (c) *the AA model;* (d) *the AA model with automatic selection of parameter;* (e) *the spatially varying parameters method;* (f) *the RLO model;* (g) *the RISS model;* (h) *the HNW model.*
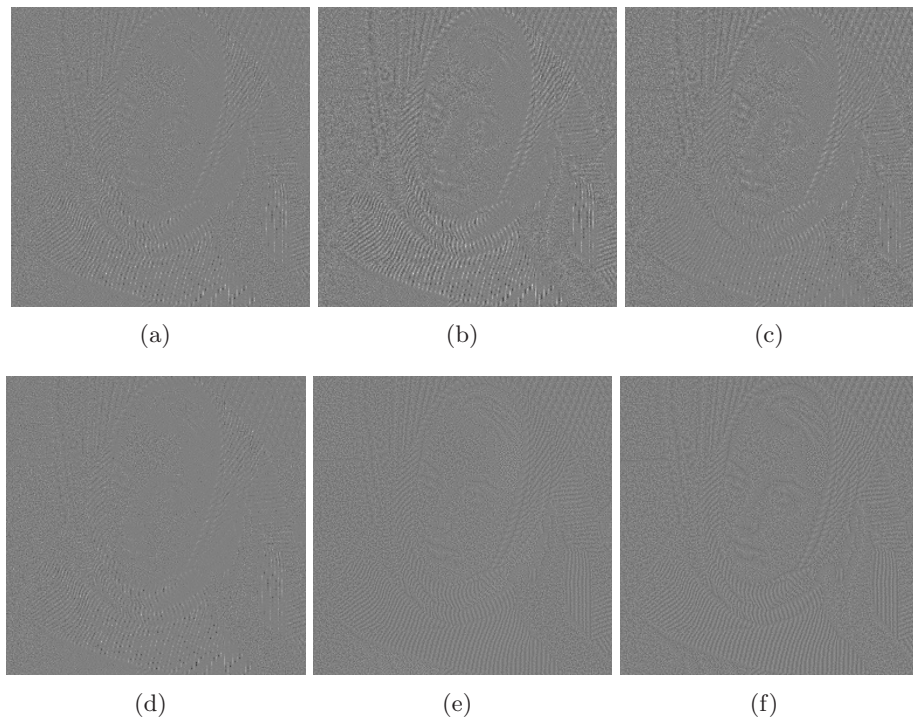
Figure 8. *The noise residue:* (a) *the AA model;* (b) *the AA model with automatic selection of parameter;* (c) *the spatially varying parameters method;* (d) *the RLO model;* (e) *the RISS model;* (f) *the HNW model.*

On the other hand, we test the influence of the radius of the Gaussian kernel K. We consider the Barbara image with Gamma noise (variance = 0.01). Let the radius of the Gaussian kernel be ω; a proper choice of window size is $4\omega+1$ (which is also used in [6]). When $\omega \geq 3$, the results are quite good. Indeed, for $\omega = 3, 7, 11, 15, 19$, and 27, the corresponding SNRs are 16.29dB, 16.10dB, 15.98dB, 15.86dB, 15.76dB, and 15.60dB. We see that as the radius ω increases, the SNR decreases slowly. Visually, we find that the recovered image loses more details as ω increases. Theoretically, as $\omega \to +\infty$, the spatially varying parameters method approximates the AA model with automatic selection of regularization parameter.

We display in Figure 9 the curves of SNRs with respect to iterations of the AA model, the AA model with automatic selection of regularization parameter, and the spatially varying parameters method for denoising images in Figures 2, 4, and 5. In comparing these curves, we see that the spatially varying parameters method is stable with higher SNRs than the other two models. We can obtain the highest SNR at convergence using the spatially varying parameters method since the SNR is a monotonic increasing function. When the iterative algorithm for using the spatially varying parameters method converges, it is a good stopping criterion for obtaining the high SNRs for the denoised images. However, we may miss the maximum SNR point when the AA model with automatic selection of regularization parameter converges since the SNR curves are concave. We also note that with some λ, the AA model gives similar results (similar SNR value and visual quality) as the AA model with automatic selection of regularization parameter, but the corresponding SNR value is lower than the optimal SNR value.
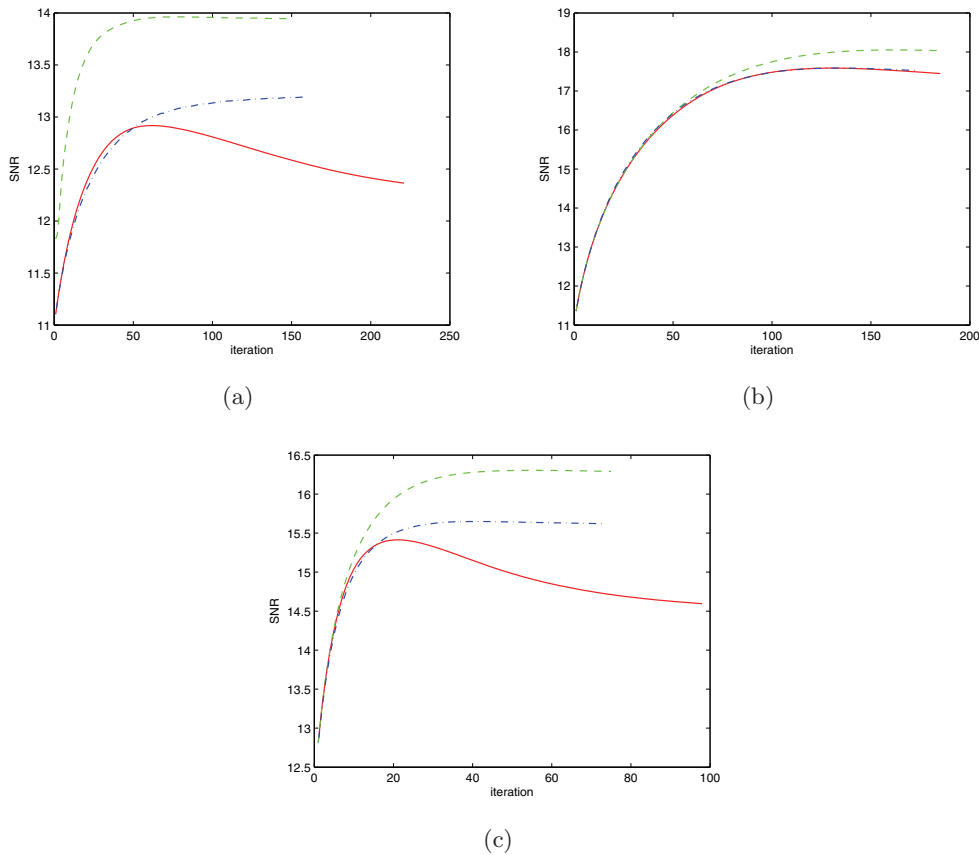
(a)

(b)

(c)

Figure 9. *The SNRs with respect to iterations by using the AA model (dash-dot line), the AA model with automatic selection of parameter (solid line), and the spatially varying parameters method (dashed line) for* (a) *Figure* 2, (b) *Figure* 4, *and* (c) *Figure* 5.

Finally, we compare the proposed methods with AA model for recovering real SAR images in Figures 10–11. Figure 10(a) is a testing image used in [3]. Figure 10(b) shows the reference image. The restoration results of the AA model, the AA model with automatic selection of regularization parameter, and the spatially varying parameters method are displayed in Figures 10(c)–10(e), respectively. We find that the spatially varying parameters method preserves the textures better than the other two models. The denoising results can also be observed in Figure 11(d), in which the textures of trees are preserved better than in Figures 11(b) and 11(c). Meanwhile, the scalar parameter model has a performance similar to that of the AA model. Note that for these two real SAR images, the variance of noise is unknown. We estimate the noise variance σ^2 by trial and error.

In summary, we have studied some basic properties of the AA variational model for multiplicative noise removal. We have developed a scalar regularization parameter model in order to choose λ automatically. We have studied the spatially varying regularization parameters method to restore textures more effectively in the denoising process. Experimental results have shown that the proposed method is quite effective.
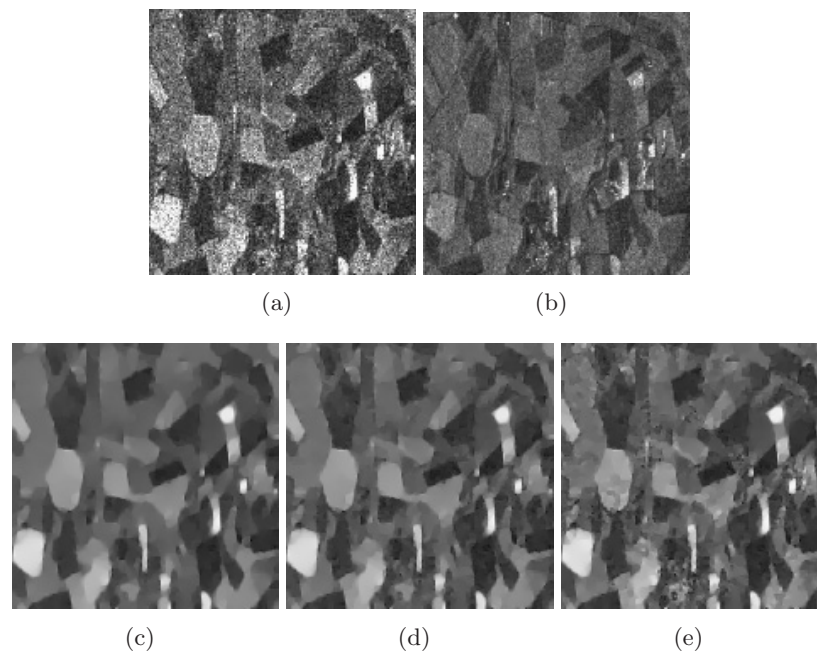
(a)   (b)

(c)   (d)   (e)

Figure 10. (a) *The original SAR image from* [3]; (b) *the reference image;* (c) *the AA model with* $\lambda = 180$; (d) *the AA model with automatic selection of parameter;* (e) *the spatially varying parameters method. The estimated variance* σ^2 *is* 0.05.
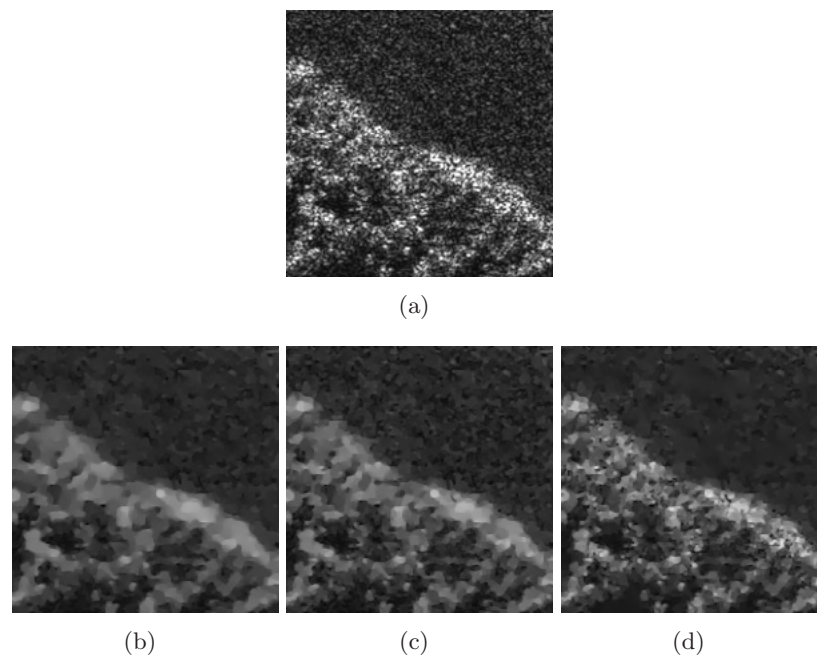

(a)

(b)   (c)   (d)

Figure 11. (a) *The original SAR image;* (b) *the AA model with* $\lambda = 100$; (c) *the AA model with automatic selection of parameter;* (d) *the spatially varying parameters method. The estimated variance* σ^2 *is* 0.08.

REFERENCES

[1] A. Almansa, C. Ballester, V. Caselles, and G. Haro, *A TV based restoration model with local constraints*, J. Sci. Comput., 34 (2008), pp. 209–236.

[2] F. Argenti and G. Torricelli, *Speckle suppression in ultrasonic images based on undecimated wavelets*, EURASIP J. Appl. Signal Process., 5 (2003), pp. 470–478.

[3] G. Aubert and J.-F. Aujol, *A variational approach to removing multiplicative noise*, SIAM J. Appl. Math., 68 (2008), pp. 925–946.

[4] M. Bertalmio, V. Caselles, B. Rougé, and A. Solé, *TV based image restoration with local constraints*, J. Sci. Comput., 19 (2003), pp. 95–122.

[5] S. Durand, J. Fadili, and M. Nikolova, *Multiplicative noise clearing via a variational method involving curvelet coefficients*, in Scale Space and Variational Methods in Computer Vision, Lecture Notes in Comput. Sci. 5567, X.-C. Tai, K. Morken, M. Lysaker, and K.-A. Lie, eds., Springer, Berlin, 2009, pp. 282–294.

[6] G. Gilboa, N. Sochen, and Y. Y. Zeevi, *Variational denoising of partly textured images by spatially varying constraints*, IEEE Trans. Image Process., 15 (2006), pp. 2281–2289.

[7] Y.-M. Huang, M. K. Ng, and Y.-W. Wen, *A new total variation method for multiplicative noise removal*, SIAM J. Imaging Sci., 2 (2009), pp. 20–40.

[8] A. Montillo, J. Udupa, L. Axel, and D. Metaxas, *Interaction between noise suppression and inhomogeneity correction in MRI*, in Proceedings of SPIE, Vol. 5032, 2003, pp. 1025–1036.

[9] L. I. Rudin, P. L. Lions, and S. Osher, *Multiplicative denoising and deblurring: Theory and algorithms*, in Geometric Level Set Methods in Imaging, Vision, and Graphics, S. Osher and N. Paragios, eds., Springer, New York, 2003, pp. 103–119.

[10] L. Rudin, S. Osher, and E. Fatemi, *Nonlinear total variation based noise removal algorithms*, Phys. D, 60 (1992), pp. 259–268.

[11] J. Shi and S. Osher, *A nonlinear inverse scale space method for a convex multiplicative noise model*, SIAM J. Imaging Sci., 1 (2008), pp. 294–321.

[12] M. Tur, C. Chin, and J. Goodman, *When is speckle noise multiplicative?*, Appl. Opt., 21 (1982), pp. 1157–1159.

[13] R. Wagner, S. Smith, J. Sandrik, and H. Lopez, *Statistics of speckle in ultrasound B-scans*, IEEE Trans. Son. Ultrason., 30 (1983), pp. 156–163.